PCCP

Prediction of the Structures and Heats of Formation of MO_2, MO_3, and M_2O_5 for M = V, Nb, Ta, Pa

Journal:	*Physical Chemistry Chemical Physics*
Manuscript ID	CP-ART-01-2023-000380.R1
Article Type:	Paper
Date Submitted by the Author:	12-Feb-2023

Complete List of Authors:	Lontchi, Eddy; The University of Alabama, Chemistry Mason, Marcos; The University of Alabama, Chemistry Vasiliu, Monica; The University of Alabama, Chemistry Dixon, David; The University of Alabama, Chemistry

Prediction of the Structures and Heats of Formation of MO_2, MO_3, and M_2O_5 for M = V, Nb, Ta, Pa

Eddy Lontchi, Marcos M. Mason, Monica Vasiliu, and David A. Dixon*

[1]Department of Chemistry and Biochemistry, The University of Alabama, Shelby Hall, Tuscaloosa AL 35487-0336, United States

Email: David A. Dixon: dadixon@ua.edu

Abstract

Mono-, di-, and tri-bridge isomers of M_2O_5 as well as those for the MO_2 and MO_3 fragments for M = V, Nb, Ta, and Pa were optimized at the density functional theory (DFT) level. Single point CCSD(T) calculations extrapolated to the complete basis set (CBS) limit at the DFT geometries were used to predict the energetics. The lowest energy dimer isomer was the di-bridge for M = V and Nb and the tri-bridge for M = Ta and Pa. The di-bridge isomers were predicted to be composed of MO_2^+ and MO_3^- fragments, whereas the mono- and tri-bridge are two MO_2^+ fragments linked by an O^{2-}. The heats of formation of M_2O_5 dimers, as well as MO_2 and MO_3 neutral and ionic species were predicted using the Feller-Peterson-Dixon (FPD) approach. The heats of formation of the MF_5 species were calculated to provide additional benchmarks. Dimerization energies to form the M_2O_5 dimers are predicted to become more negative going down group 5 and range from -29 to -45 kcal/mol. The ionization energies (IEs) for VO_2 and TaO_2 are essentially the same at 8.75 eV whereas the IEs for NbO_2 and PaO_2 are 8.10 and 6.25 eV, respectively. The predicted adiabatic electron affinities (AEAs) range from 3.75 eV to 4.45 eV for the MO_3 species and vertical detachment energies from 4.21 to 4.59 eV for MO_3^-. The calculated M=O bond dissociation energies increase from 143 kcal/mol for M = V to ~ 170 kcal/mol for M = Nb and Ta to ~ 200 kcal/mol for M = Pa. The M-O bond dissociation energies are all similar

ranging from 97 to 107 kcal/mol. A natural bond analysis provided insights into the types of chemical bonds in terms of their ionic character. Pa_2O_5 is predicted to behave like an actinyl species dominated by the interactions of approximately linear PaO_2^+ groups.

Introduction

A fundamental understanding of the bonding, energetics, and structures of transition metal clusters can provide insights into their unique chemical properties. There is broad interest in the chemistry of transition metal oxide due to the potential use of these oxides in catalytic, magnetic, optical, electrochemical, and energy storage applications.[1,2] As an example, vanadium oxide catalysts are used for a number of important reactions, including the oxidation of methanol,[3] industrial sulfuric acid production, and the removal of NO_x pollutants from combustion processes via the selective catalytic reduction (SCR) reactions.[4,5,6] Small vanadium oxide clusters have been used to model a range of catalytic activities[7,8,9] using structures based on a combined NMR and computational determination of the structures of the supported clusters.[10,11] Oxides of niobium and tantalum have received attention in high temperature chemistry and for optical applications.[12,13,14] In many, if not most of their applications, group 5 oxides are employed as a single surface layer deposited on a support material often as M_2O_5. Group 5 oxides are known to show a high degree of polymorphism and variability in oxygen composition, and vanadium oxides in particular reversibly lose oxygen on heating.[15] Studies of Nb_2O_5 and Ta_2O_5 have mainly focused on their properties in condensed phases.[16,17,18,19]

The protactinium oxides are not as well explored as the group 5, (V, Nb, and Ta) oxides. Pa shares a pentavalent oxidation state, but the ground state of Pa is the $5f^26d^17s^2$ configuration allowing for f and d orbital chemistry as compared to the ns^2md^3 valence configuration for the group 5 transition metals. Pa plays an important role in the nuclear enterprise.[20] A previous study

of the role of 5f and 6d orbitals of actinide oxides in the bulk showed that Pa is the point at which the f and d orbital cross energetically.[21] Wilson et al.[22] explored the potential behavior of Pa as being transition metal-like via synthesis and bonding analysis of a Pa peroxo-cluster, and determined that the valence population of Pa is roughly the same in the 5f and 6d orbitals compared to later actinides. Recent theoretical studies have explored the crystallographic phases of Pa_2O_5. Siberchicot and Aupiais[23] performed density functional theory (DFT) calculations on various crystallographic phases of Pa_2O_5 to predict their electronic structure. Liu et al.[24] performed similar DFT calculations to predict the structure of Pa_2O_5 based on the crystallographic phases of V_2O_5, Nb_2O_5, and Ta_2O_5. Liu et al.[25] extended their investigations to Pa_2O_5 structures formed from the fluorite structure.

As studies into the gas-phase structure and properties of the group 5 M_2O_5 species have not been as broadly explored as their chemistry in other phases, [26] it is important to gain further insights into their properties. Vyboishchikov et al. performed DFT calculations for three V_2O_5 isomers and predicted the di-bridge isomer to be the most stable isomer with the mono-bridge higher by 16.5 (69 kJ/mol) and 18.6 (78 kJ/mol) kcal/mol with the B3LYP and BP86 functionals, respectively.[27,28] The tri-bridge V_2O_5 isomer was the least stable and was predicted to be a higher order saddle point that without symmetry constraints optimized to the di-bridge isomer. Calatayud et al.[29] similarly found three isomers of neutral and anionic V_2O_5 at the DFT/B3LYP level, with the tri-bridge structure as a saddle point 6.9 kcal/mol higher in energy than the di-bridge isomer. Kovács has recently summarized the properties of high valent actinides oxide dimers starting at U.[30]

As part of our efforts[31,32,33,34,35,36,37] to understand the structure and reactivity of transition metal oxide compounds and how they compare with the actinides, we have predicted the structures and energetics of M_2O_5 for M = V, Nb, Ta, and Pa using computational chemistry methods based

on the Feller Peterson Dixon (FPD) composite correlated molecular orbital theory approach.[38,39,40,41,42] In addition, we have used this same approach to predict the energetics for $MO_2^{0/+}$ and $MO_3^{0/-}$ which are important fragments. The current results substantially extend the available reliable energetic information on these metal oxides.

Computational Methods

Geometry optimizations and vibrational frequency calculations were calculated at the DFT[43] level using the hybrid exchange-correlation functional B3LYP.[44,45,46] These calculations use the correlation consistent basis sets aug-cc-pVDZ for H, O, and F[47,48,49] and the aug-cc-pVDZ-PP basis sets for the group 5 metals[50,51,52,53,54] and cc-pVDZ-PP for Pa.[54] The effective core potentials (ECPs) include 10 electrons in the 1s2s2p orbitals for V, 28 electrons in the 1s2s2p3s3p3d orbitals for Nb, and 60 electrons in the 1s2s2p3s3p3d4s4p4d4f orbitals for Ta and Pa. Frequency calculations were used to calculate the zero-point energy (ΔE_{ZPE}) to obtain thermodynamic energies, described below. DFT calculations were performed using Gaussian 16.[55]

To calculate the total atomization energies and reaction energies, a series of single point calculations at the DFT optimized geometries were performed at the CCSD(T) (coupled cluster with single and double excitation with a perturbative triples correction) level.[56,57,58,59] The Kohn-Sham PW91[60,61,62] orbitals were used for the correlation calculations as these can provide better orbitals in terms of the initial correlation effects.[36,37] The open-shell calculations were done with the R/UCCSD(T) approach, where a restricted open-shell Hartree-Fock (ROHF) calculation using the PW91 orbitals was performed and the spin constraint was then relaxed in the coupled-cluster calculation.[63,64,65] Results with the HF orbitals are given in the Supporting Information. Correlation consistent basis sets with the appropriate ECPs were used in all CCSD(T) calculations. Other

calculations were performed for some specific clusters and are discussed in detail next. CCSD(T) calculations were performed in Molpro 2021.1.[66,67,68]

The total atomization energies (TAEs, or ΣD_0) for M_2O_5, $MO_2^{0/+}$, $MO_3^{0/-}$, $MO_2(OH)$, and MF_5 (M = V, Nb, Ta) were calculated relative to the ground state atoms following the FPD composite approach as given in equation (1).

$$\Sigma D_0 = \Delta E_{CBS} + \Delta E_{ECP} + \Delta E_{SO} + \Delta E_{ZPE} \quad (1)$$

ΔE_{CBS} is the TAE calculated at the double, triple and quadruple ζ basis set level and extrapolated to the complete basis set (CBS) limit by means of a 3-point extrapolation as defined by equation (2),[69]

$$E_n = E_{CBS} + A \exp[-(n-1)] + B \exp[-(n-1)^2] \quad (2)$$

where n represents the level of the basis set.

For M = V, CBS calculations were performed using the third-order Douglas-Kroll-Hess (DKH3) Hamiltonian[70,71,72] with the relativistic aug-cc-pwCVnZ-DK (n=D,T,Q)[73,74] basis sets including weighted core-valence correlation functions.[75] Correlation of the outer core electrons was included in the calculations and the 1s2s2p orbitals of V were frozen. Additional calculations were performed for VF_5 with the aug-cc-pwCVnZ basis sets for F and a weighted core ECP for V. For M = Nb and Ta, CBS calculations were performed using the aug-cc-pwCVnZ basis sets for O and F, and the aug-cc-pwCVnZ-PP basis sets for Nb and Ta for n = D, T, Q. For molecules containing H, the aug-cc-pVnZ basis set was used.[48] The remaining terms in equation (1) are additive corrections to the CBS TAE.

The ΔE_{ECP} term, the correction for use of an effective core potential, was calculated as the difference in TAE between calculations with valence basis sets and scalar relativistic calculations with the DKH3 Hamiltonian at the triple ζ level. For molecules containing Nb, the cc-pwCVTZ-

PP basis sets was used for Nb and the aug-cc-pwCVTZ basis for O or F. The DKH3 Hamiltonian calculations used the aug-cc-pwCVTZ-DK basis sets, and the O 1s or F 1s was correlated in the calculations. For Ta molecules, the aug-cc-pwCVTZ basis set for O with O 1s correlated and cc-pwCVTZ-PP basis set for Ta were used. The DKH3 Hamiltonian calculations were performed using the aug-cc-pwCVTZ-DK basis set for O where the O 1s was correlated and the cc-pwCVTZ-DK with additional high angular momentum functions to correlate the Ta 4f orbitals[52]. Scalar relativistic corrections are implicitly included in the CBS calculations with V.

ΔE_{SO} are the atomic spin orbit corrections. Spin orbit corrections for the atoms were obtained by state averaging of the experimental values:[76,77,78] ΔE_{SO} (V) = -0.91, ΔE_{SO} (Nb) = -1.81, ΔE_{SO} (Ta) = -10.2, ΔE_{SO} (O) = -0.22, and ΔE_{SO} (F) = -0.39 kcal/mol. Molecular spin orbit coupling effects were not calculated as they were assumed to be negligible for the closed shell species studied in the present work. The ΔE_{ZPE} term is the molecular zero-point energy vibration calculated at the DFT/B3LYP level.

As it is difficult to calculate the energy of the ground state of the Pa atom, the atomization energy was calculated relative to the Pa^+ ground state ($7s^25f^2$) and corrected to the ground state of Pa ($7s^25f^26d^1$) by the experimental ionization energy of Pa 135.8 ± 2.8 kcal/mol.[79] The calculations for the Pa compounds were performed at the CCSD(T)/cc-pwCV*n*Z-DK (n = D, T, Q) level of theory with the DKH3 Hamiltonian. The 5s5p5d6s6p7s5f6d electrons were correlated. Additional calculations for PaF_5 were performed with cc-pwCV*n*Z-pp for Pa.[53,54] The atomic spin-orbit corrections (ΔE_{SO}) are ΔE_{SO} (O) = -0.22 and ΔE_{SO} (Pa^+) = -13.9 kcal/mol.[78] Molecular spin orbit corrections for the open shell species are ΔE_{SO} (PaO_3) = -0.6 kcal/mol and ΔE_{SO} (PaO_2) = -1.5 kcal/mol. The spin-orbit corrections for Pa^+, PaO_2, and PaO_3 were obtained at the SO-CASPT2/DK level[80,81,82,83] with the cc-pVQZ-DK basis set for Pa^+ and cc-pVDZ-DK basis set for PaO_2, and

PaO_3. These spin-orbit calculations were done following the state interacting approach we have previously used.[84,85,86]

Heats of formation at 0 K were calculated by combining the computed ΣD_0 values with the experimentally known enthalpies of formation at 0 K for the elements. The values for $\Delta H_{f,0K}$ (O) = 59.00, $\Delta H_{f,0K}$ (H) = 51.63, and $\Delta H_{f,0K}$ (F) = 18.47 kcal/mol are from the active thermochemical tables (ATcT).[87,88,89] The values for the transition metals are $\Delta H_{f,0K}$ (V) = 122.4 ± 1.9, $\Delta H_{f,0K}$ (Nb) = 174.4 ± 1.9, and $\Delta H_{f,0K}$ (Ta) = 186.8 ± 0.5 kcal/mol from the JANAF Tables.[90] The heats of formation of the transition metals are consistent with the values from Yungman et al.[91] of $\Delta H_{f,0K}$ (V) = 122.2 ± 1.0, $\Delta H_{f,0K}$ (Nb) = 172.0 ± 1.0, and $\Delta H_{f,0K}$ (Ta) = 187.8 ± 1.0. The value for $\Delta H_{f,0K}$ (Pa) = 136.2 ± 2.4 kcal/mol is from Konings et al.[92] where we use the thermal correction from 298 to 0 K from Yungman et al.[91] This more recent value differs from the older values of $\Delta H_{f,0K}$ (Pa) = 145 ± 5 kcal/mol from Yungman et al.[91] and the value of 145.1 kcal/mol from Wagman et al.[93] Heats of formation at 298 K were calculated using molecular thermal corrections obtained from the DFT calculations, thermal corrections for the atoms (H = 1.01,[94] O = 1.04,[94] F = 1.05,[94] V = 1.110,[91] Nb = 1.255 ± 0.05,[91] Ta = 1.3617 ± 0.05,[91] and Pa = 1.54 ± 0.10[91] kcal/mol) and the calculated heats of formation at 0 K following the procedures of Curtiss et al.[94] Total atomization energies and the corresponding heat of formation were calculated for the M_2O_5 mono-bridge isomers as these have the simplest electronic structure. The thermochemistry values for the di- and tri-bridge isomers were calculated based on their energies relative to the mono-bridge isomer.

Results and Discussion

MO_2 and MO_3 Geometries Before discussing the geometries of the M_2O_5, we discuss the geometries of the corresponding neutral and ionic MO_2 and MO_3 fragments. MO_2 and MO_2^+ were optimized at the DFT/B3LYP level and the geometry parameters are shown in Figure 1. The formal

oxidation state for M in MO_2 and MO_2^+ fragments is +IV and +V, respectively. For M = V, Nb, and Ta, the MO_2 and MO_2^+ species are bent with shorter bonds and smaller ∠O-M-O predicted for the cations. The DFT geometries of PaO_2 and $PaO_2(OH)$ has been previously reported.[95] At their ground states, PaO_2 and PaO_2^+ were both predicted to be linear, with a slightly shorter Pa-O bond in the cation. The major difference in the structures of the group 5 $MO_2^{0/+}$ (M = V, Nb, Ta) and the actinide $PaO_2^{0/+}$ can be attributed to the presence of the f orbital and the stability of the actinyl moiety. Similar differences were predicted for the group 6 MO_2 and MO_2^+ (M = Mo, W) and U metal oxide species, where the transition metal MO_2 and MO_2^+ (M = Mo, W) were predicted to have a bent C_{2v} structure, whereas UO_2 and UO_2^+ were both predicted to be linear.[96]

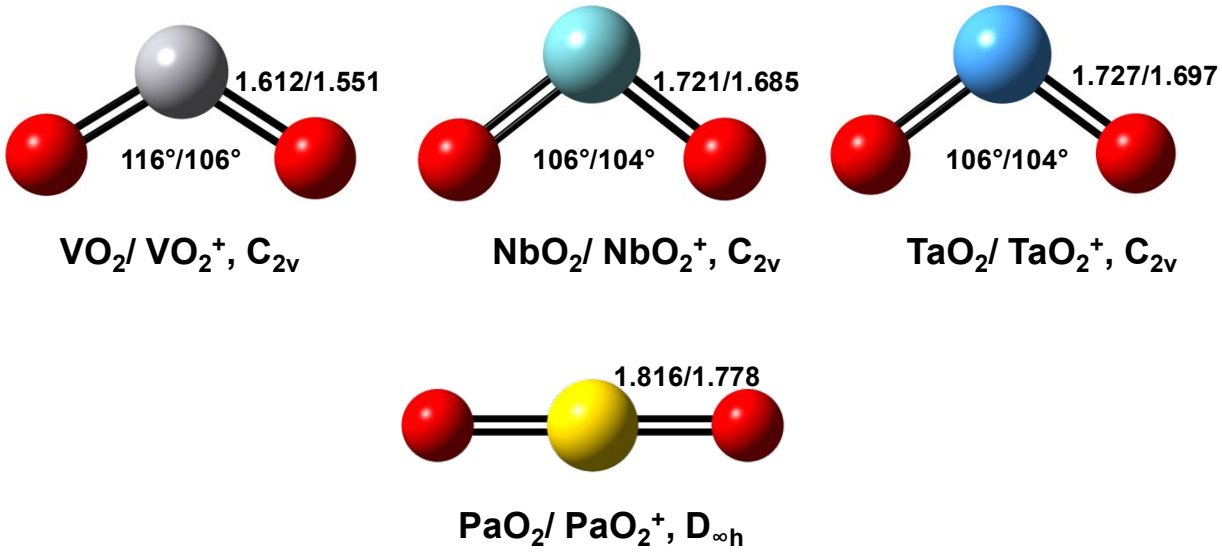

Figure 1. Optimized geometries for MO_2 and MO_2^+, M = V, Nb, Ta, and Pa, species. O atoms in red, V atoms in silver, Nb atoms in teal, Ta atoms in blue, and Pa atoms in gold.

The optimized geometries for MO_3 and MO_3^- at the DFT/B3LYP level are shown in Figure 2, with M in the formal +V oxidation state. The MO_3 radicals for M = V, Nb, and Ta are pyramidal

in C_s symmetry, with one long M-O bond and two equivalent short M-O bonds. The addition of an electron to form the closed shell MO_3^- for M = V is planar with D_{3h} symmetry and for M = Nb, Ta, and Pa is pyramidal with C_{3v} symmetry. The planar D_{3h} MO_3^- for M = Nb and Ta have respective imaginary frequencies of 70*i* cm^{-1} and 112*i* cm^{-1} at the DFT/B3LYP level, with respective inversion barriers of 0.21 and 1.77 kcal/mol at the CCCDS(T)/cc-pVTZ-DK level.

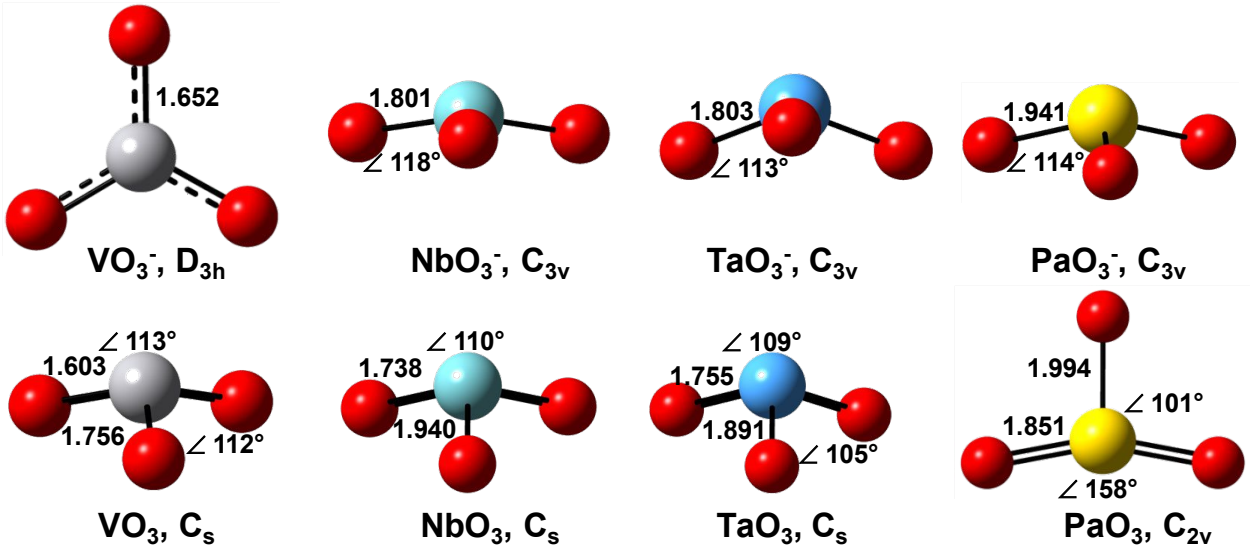

Figure 2. Optimized geometries for MO_3 and MO_3^- , M = V, Nb, Ta, and Pa, species. O atoms in red, V atoms in silver, Nb atoms in teal, Ta atoms in blue, and Pa atoms in gold.

The structure of PaO_3 is derived from PaO_2, where the addition of an equatorial O bends the actinyl-like moiety by 22° and slightly lengthens the bond of the axial groups, giving a planar C_{2v} structure. The planar D_{3h} structure of PaO_3^- is a transition state with an imaginary frequency of 94*i* cm^{-1} at the DFT/B3LYP level and an inversion barrier of 3.0 kcal/mol at the CCCDS(T)/cc-pVTZ-DK level. The planar C_{2v} structure for PaO_3^-, with one short M-O bond and two slightly longer M-O bonds, is also a transition state with a similar imaginary frequency of 92*i* cm^{-1} at the

DFT/B3LYP level. Optimized geometries for $MO_2(OH)$ and MF_5 are discussed in the Supporting Information for reactions discussed below.

M_2O_5 Geometries Three stable isomers were predicted for the M_2O_5 molecules, the mono-, di-, and tri-bridge O structures, with the relative isomer energies in Table 1 and structures for V_2O_5 and Nb_2O_5 in Figure 3 and for Ta_2O_5 and Pa_2O_5 in Figure 4. For M = V, as previously reported,[27,28]

Table 1. Relative Isomer Enthalpies at 298 K (ΔH, kcal/mol) at the CCSD(T)/CBS Level.

M_2O_5	Isomer	Symmetry	ΔH_{298K}
V_2O_5	di-bridge	C_s	0.0
	tri-bridge	C_1	6.9
	mono-bridge	C_2	22.4
Nb_2O_5	di-bridge	C_s	0.0
	tri-bridge	D_{3h}	2.7
	mono-bridge	C_2	23.9
Ta_2O_5	tri-bridge	D_{3h}	0.0
	di-bridge	C_s	6.7
	mono-bridge	C_2	36.3
Pa_2O_5	tri-bridge	C_2	0.0
	di-bridge	C_s	12.7
	mono-bridge	D_{2d}	34.2

the lowest energy isomer was predicted to be the di-bridge followed by the tri-bridge and then the mono-bridge. The ground state di-bridge isomer is best described as an ionic complex of MO_3^- and MO_2^+ (Figure 3). The MO_3^- moiety is connected to the MO_2^+ fragment by bonds that are 0.3 Å longer than the M-O bonds in the anion fragment. The two V=O bond distances in the MO_2^+ fragment are comparable to the V=O bond distance in the MO_3^- fragment. The tri-bridge isomer is a distorted di-bridge, where the MO_3^- and MO_2^+ fragments are rotated/tilted inward, toward the bridge. The mono-bridge isomer with C_2 symmetry is best described as two MO_2^+ fragments linked together by an O^{2-}. The $\angle$V-O_{br}-V is bent by < 20° from linearity. Mass spectrometry studies on

the composition of group 5 M_2O_5 ionic clusters shows that fragmentation leads to such MO_2 and MO_3 fragments,[97,98] consistent with the above analysis and for the analysis described below.

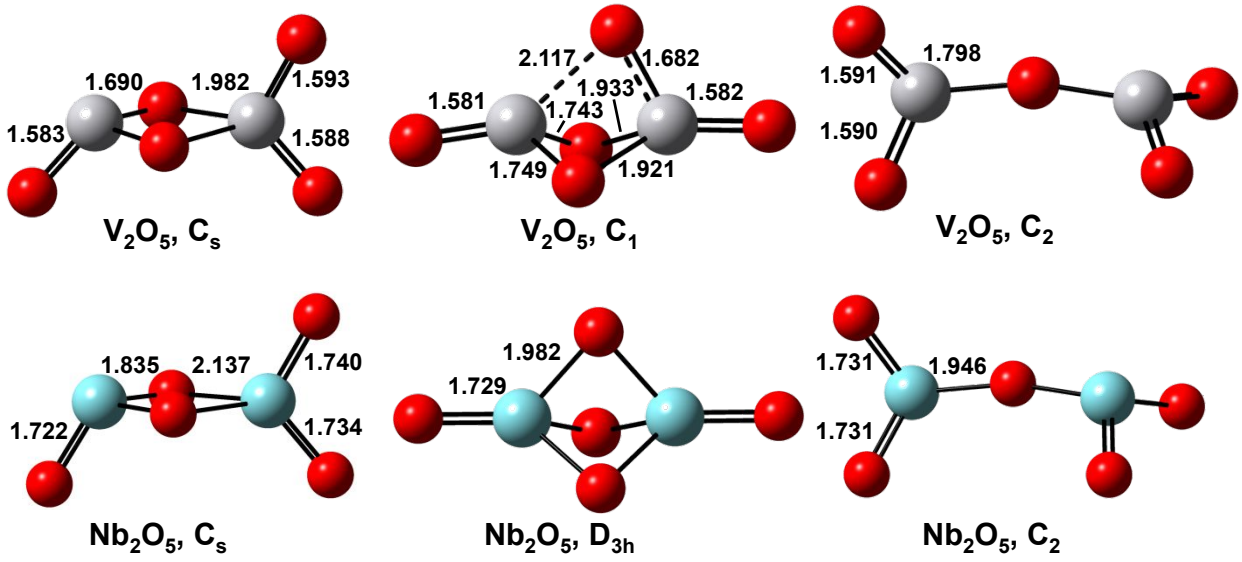

Figure 3. DFT optimized structures for V_2O_5 and Nb_2O_5 isomers. O atoms in red, V atoms in silver and Nb atoms in teal.

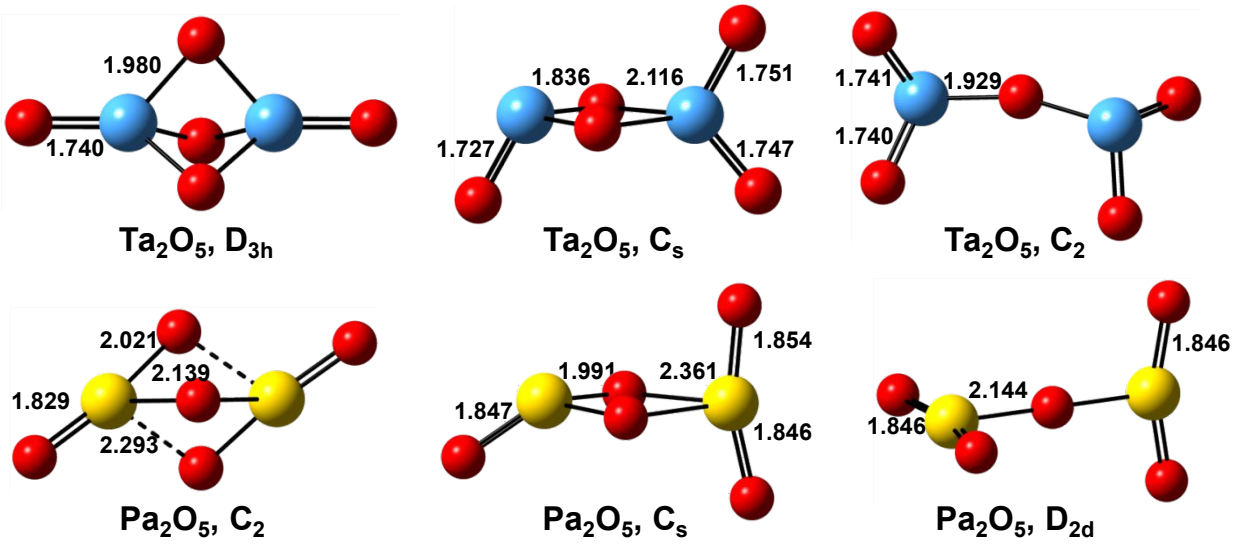

Figure 4. DFT optimized structures for Ta_2O_5 and Pa_2O_5 isomers. O atoms in red, Ta atoms in blue, and Pa atoms in gold.

Similarly, for M = Nb, the lowest energy isomer was predicted to be the di-bridge with the tri-bridge isomer less than 3 kcal/mol higher in energy; the mono-bridge isomer is again the least stable isomer. As described above for the V_2O_5 di-bridge isomer, the Nb_2O_5 di-bridge isomer is best described as an ionic complex of NbO_3^- and NbO_2^+ (Figure 3). The bond distances in the di-bridge isomer follow the same pattern as for the V_2O_5 di-bridge isomer. The tri-bridge isomer has D_{3h} symmetry and the Nb-O_{br} bond distances are the average of the two unique Nb-O distances in the di-bridge isomer. Similar to the V mono-bridge isomer, the Nb mono-bridge isomer has two NbO_2^+ fragments connected by a bridging O^{2-}. The Nb=O bond distances in the mono-bridge isomer are essentially the same as the Nb=O bonds in the other two isomers. Thus, the Nb=O and Nb-O bond distances do not substantially vary in the three isomers.

In contrast to the Nb and V oxide dimers, for M = Ta the lowest energy isomer is predicted to be the tri-bridge isomer. The di-bridge isomer is the next highest in energy and the mono-bridge isomer is again the least stable. The geometry of the tri-bridge Ta_2O_5 isomer is essentially identical to the tri-bridge Nb_2O_5 isomer. Again, the di-bridge isomer can be described as the binding of TaO_3^- and TaO_2^+ and is almost identical to that of the corresponding Nb_2O_5 isomer. The bonds connecting the two fragments are slightly shorter in the Ta isomer as compared to the Nb isomer. The highest energy mono-bridge isomer is essentially the same as the Nb isomer, with two TaO_2^+ fragments connected by an O^{2-} and an $\angle$Ta-O_{br}-Ta of 163°.

The lowest energy isomer of Pa_2O_5 was predicted to be the tri-bridge. The di-bridge isomer is the next highest in energy and the mono-bridge isomer is again the highest in energy. The tri-bridge isomer has lower symmetry than found for Nb and Ta and the Pa=O bonds are no longer on the same axis. The Pa_2O_5 tri-bridge isomer can be described as connecting two PaO_2^+ fragments

with an O^{2-}. However, one of the Pa-O bonds in the PaO_2^+ actinyl fragment becomes elongated on bonding to the other Pa. The $\angle O_{term}$-Pa-O_{term} in the PaO_2^+ fragments deviate from linearity by < 10°. This type of bonding can be described as a side-on cation-cation interaction moderated by the additional O^{2-} bridging oxygen.[99,100] This type of cation-cation interaction has been observed for NpO_2^+- NpO_2^+.[100] This structure is not predicted for the transition metal species due to the fact that the MO_2^+ fragment for the transition metals is bent and does not have actinyl type character. The di-bridge isomer is a complex of PaO_3^- and PaO_2^+ molecules, consistent with the group 5 dimers. The PaO_2^+ fragment maintains its actinyl character and the $\angle O_{term}$=Pa=O_{term} deviates by < 20° from linearity. The mono-bridge isomer can be described as two PaO_2^+ molecules bridged by an O^{2-}. The PaO_2^+ groups are clearly actinyl-like with an $\angle$ O_{term}=Pa=O_{term} deviating from linearity by < 20° and the two groups perpendicular to each other. In this case the $\angle$Pa-O_{br}-Pa is linear.

Heats of Formation: Fragments As the heats of formation of the M_2O_5 are not available from experiment, we first discuss the heats of formation of the MO_2 and MO_3 species where some experimental and additional computational data is available. The TAEs and gas-phase heats of formation for the bare ionic fragments and the corresponding neutrals as well as for MO_2(OH) species have been calculated using the FPD approach (Table 2). The calculated heats of formation with a single V or Nb atom have an estimated error of ± 3 kcal/mol as the atomic heat of formation introduces an error of ± 2 kcal/mol. For a single Ta, the error bar is on the order of ± 2 kcal/mol as the error for the atomic heat of formation is smaller. For the compounds with a single Pa, the error is on the order of ± 4 kcal/mol due to the error bars on the heat of formation of the Pa atom of ± 2.4 kcal/mol. We estimate that the errors in the calculated heats of formation for the compounds with two V or two Nb to be on the order of ± 5 kcal/mol and with two Ta atoms to be ± 3 kcal/mol.

The error bars for the calculated heats of formation of the compounds with two Pa atoms are on the order of at least ± 6 kcal/mol.

Table 2. Total Atomization Energies and Heats of Formation at 0 K and 298K at the CBS Level in kcal/mol for MO_2, MO_2^+, MO_3, MO_3^-, and $MO_2(OH)$ for M = V, Nb, Ta, and Pa.

Species	ΣD^0_{0K}	$\Delta H_{f,0K}$	$\Delta H_{f,298K}$	$\Delta H_{f,298K}$ **expt**
VO_2	286.8	-46.5	-46.9	-55.6 ± 10[90] -56.9[93]
VO_2^+	85.3	155.1	154.5	
VO_3	383.0	-83.6	-83.3	
VO_3^-	473.8	-174.4	-174.2	
$VO_2(OH)$	490.1	-139.1	-138.5	
NbO_2	337.2	-44.8	-45.5	-47.8 ± 5[90]
NbO_2^+	150.7	141.8	141.1	
NbO_3	431.2	-79.8	-80.6	
NbO_3^-	524.0	-172.6	-173.4	
$NbO_2(OH)$	546.6	-143.6	-145.1	
TaO_2	342.4	-37.6 (-38.5)[a]	-38.4 (-39.2)[a]	-48.0 ± 15[90] -41.1 ± 15[93] -46.2 ± 4.5[105]
TaO_2^+	140.6	164.1	163.3	
TaO_3	431.7	-68.0	-68.8	
TaO_3^-	534.4	-170.6	-171.7	
$TaO_2(OH)$	555.0	-139.6	-141.3	
PaO_2[b]	400.0	-145.8	-144.8	-122.7 ± 4.0[107] -122.6 ± 18[106]
PaO_2^+	390.2	-0.1	-0.7	13.6 ± 14[106]
PaO_3[c]	486.9	-173.7	-174.4	
PaO_3^-[d]	573.5	-260.3	-261.2	
$PaO_2(OH)$[e]	609.9	-245.1	-246.6	

[a] Values in parentheses at the CBS Q5 limit. [b-e] Atomization energy calculated as [b]$PaO_2 \rightarrow Pa^+ + 2O$, [c]$PaO_3 \rightarrow Pa^+ + 3O$, [d]$PaO_3^- \rightarrow Pa^+ + 3O$, [e]$PaO_2(OH) \rightarrow Pa^+ + 3O + H$, and corrected by IE(Pa).

Our calculated heat of formation for VO_2 is ~ 9 kcal/mol less negative than the experimental[90] value, but within the ± 10 kcal/mol experimental error, especially considering the estimated computational error of at least ± 3 kcal/mol. Our calculated value for NbO_2 is again less

negative than the experimental value and falls within the experimental[90] error bar of ± 5 kcal/mol and the computational error bar of ± 3 kcal/mol. With a known crystalline heat of formation, for $\Delta H(NbO_2)$ = -190.0 ± 2[90] kcal/mol, the corresponding cohesive energy is 144.5 kcal/mol. Although these materials are not molecular solids, we define the cohesive energy as the energy to make a gaseous molecule with the same stoichiometry as that of the solid as this provides a base to compare different systems.[101]

Previously, Bauschlicher et al. [102] calculated the heats of formation of various tantalum oxide and tantalum oxyhydroxide species at the CCSD(T)/CBS Q5 level of theory with aug-cc-pV*n*Z basis set for O and cc-pwCV*n*Z-pp basis set for Ta (n = T, Q, and 5). For TaO_2, Bauschlicher et al. used the energy of reaction (3):

$$Ta + O_2 \rightarrow TaO_2 \quad (3)$$

The value reported by Bauschlicher et al.[102] included a ZPE and spin-orbit correction, but no pseudopotential correction. A comparison of their 0 K heats of formations values and our values at selected CBS limits are presented in Table 3. Additional comparisons at different CBS limits with calculated ΔE_{ECP} corrections are presented in the Supporting Information.

In order to better compare to the work of Bauschlicher et al., we also calculated the heat of formation using a CBS Q5 extrapolation of the form given by equation (4).[103,104]

$$E_n = E_{CBS} + A(n + 1/2)^{-4} \quad (4)$$

The agreement between the two extrapolated values is within 1 kcal/mol. For reaction (3) with the HF orbitals, we are within 0.6 kcal/mol of their value. The ΔE_{ECP} for reaction (3) is 3.0 kcal/mol which would reduce the Bauschlicher et al. value to $\Delta H_{f,0K}$ = -37.3 kcal/mol. Our corresponding $\Delta H_{f,0K}$ derived from the atomization energy with ΔE_{ECP} included is 1.4 kcal/mol less negative using the HF orbitals and the Q5 extrapolation. The value for $\Delta H_{f,0K}$ using the PW91 orbitals and

the Q5 extrapolation with the ΔE_{ECP} correction is 1.2 kcal/mol more negative and with the DTQ extrapolation is 0.3 kcal/mol more negative as compared to the prior work. Our values are all consistent with the ECP corrected results from Bauschlicher et al.[102] The calculated values for $\Delta H_{f,298K}$ (TaO_2) falls within the large experimental error bars.[90,93] Smoes et al.[105] reported a TaO_2 heat of formation with smaller error bars that is ~ 8 kcal/mol more negative than our calculated value and is not likely to be correct.

Table 3. Enthalpies ($\Delta H_{,0K}$) for Reactions (3), (5) and (6) in kcal/mol for Determination of the Heats of Formation of TaO_2 and $TaO_2(OH)$.

Method		**HF**	**PW91**
TaO_2			
$Ta + 2O \rightarrow TaO_2$	DTQ + ECP	-35.1	-37.6
$Ta + 2O \rightarrow TaO_2$	Q5 + ECP	-35.9	-38.5
$Ta + O_2 \rightarrow TaO_2$	Q5	-39.7	-42.3
$Ta + O_2 \rightarrow TaO_2$	Q5 + ECP	-36.7	-39.3
$Ta + O_2 \rightarrow TaO_2$ [a]	Q5	-40.3	
$Ta + O_2 \rightarrow TaO_2$ [b]	Q5 + ECP	-37.3	
$TaO_2(OH)$			
$Ta + 3O + H \rightarrow TaO_2(OH)$	DTQ + ECP	-139.9	-139.6
$Ta + 3O + H \rightarrow TaO_2(OH)$	Q5 + ECP	-140.5	-140.2
$Ta + O_2 + H_2O \rightarrow TaO_2(OH) + H$	Q5	-145.1	-144.7
$Ta + O_2 + H_2O \rightarrow TaO_2(OH) + H$	Q5 + ECP	-141.5	-141.1
$Ta + 3H_2O \rightarrow TaO_2(OH) + 5H$	Q5	-144.6	-144.2
$Ta + 3H_2O \rightarrow TaO_2(OH) + 5H$	Q5 + ECP	-141.4	-140.9
$Ta + O_2 + H_2O \rightarrow TaO_2(OH) + H$ [a]	Q5	-146.0	
$Ta + O_2 + H_2O \rightarrow TaO_2(OH) + H$ [b]	Q5 + ECP	-142.4	
$Ta + 3H_2O \rightarrow TaO_2(OH) + 5H$ [a]	Q5	-145.1	
$Ta + 3H_2O \rightarrow TaO_2(OH) + 5H$ [b]	Q5 + ECP	-141.8	

[a] Ref. 102. [b] Value from Ref. 102 corrected by current ΔE_{ECP}.

A similar comparison can be made for $TaO_2(OH)$ with the work of Bauschlicher et al.[102] who used reactions (5) and (6)

$$Ta + O_2 + H_2O \rightarrow TaO_2(OH) + H \quad (5)$$

$$Ta + 3H_2O \rightarrow TaO_2(OH) + 5H \quad (6)$$

The ΔE_{ECP} corrections for reactions (5) and (6) are 3.6 kcal/mol and 3.3 kcal/mol, respectively. Our final value for $\Delta H_{f,0K}$ based on the atomization energies and the PW91 orbitals is about 2 kcal/mol less negative than the corrected values using reactions (5) and (6) from Bauschlicher et al.[102] Again, the DTQ extrapolation gives a heat of formation that is about 0.6 kcal/mol less negative than the Q5 extrapolation (Supporting Information). Overall, the heats of formation calculated with the PW91 orbitals are closer to experiment than those calculated with the HF orbitals (SI) for the transition metal MO_2 species.

The calculated gas-phase heat of formation of PaO_2 with an error bar of ± 4 kcal/mol overlaps the experimental range of Marçalo and Gibson[106] values with an error bar of ± 18 kcal/mol. Our value is not consistent with the value from Kleinschmidt and Ward[107] who reported a value of -122.7 ± 4.0 kcal/mol. The latter value[107] was obtained by assuming that the heat of sublimation of PaO_2 is due only to the loss of molecular PaO_2 from the solid, but they do observe PaO in the vapor as well, suggesting a complex system, as there is also the potential for loss of O_2. We suggest that the experimental heat of formation of PaO_2 needs to be revisited. Our heat of formation for PaO_2^+ with an error bar of ± 4 kcal/mol is consistent with that of Marçalo and Gibson within the ± 14 kcal/mol error bar.[106]

The adiabatic ionization energies and electron affinities of some of the MO_2 and MO_3 species are also available from experiment. Calculated ionization energies (IEs) of the MO_2 species obtained from the difference in 0 K heats of formation between the optimized neutral and optimized cation structures are shown in Table 4 and compared to the available experimental data. The calculated VO_2 IE is approximately 4 eV lower than the experimental value of Bennet et al.[108] and 1.2 eV lower than the experimental value of Farber et al[109]. The calculated IE(PaO_2) is larger

than the experimental value of 5.9 eV[106] by 0.4 eV and is outside the range of the experimental error bar of ± 0.2 eV. Among the MO_2 species in this study, Pa has the lowest IE, followed by Nb, V, and Ta.

Table 4. Ionization Energy (IE) of MO_2 at the FPD Level in eV.

MO_2	Calc	Experiment
VO_2	8.74	12.7 ± 0.2[108] 10.0 ± 0.2[109]
NbO_2	8.09	
TaO_2	8.75	
PaO_2	6.32	5.9 ± 0.2[106]

The adiabatic electron affinity (AEA) of the MO_3 species obtained from the difference in the 0 K heats of formation between the optimized neutral and anion structures are shown in Table 5. The MO_3 species have fairly large AEAs, indicating the high stability of the closed shell anions against electron loss. TaO_3 has the largest AEA followed by NbO_3 which has an AEA that is ~ 0.4 eV smaller. The VO_3 and NbO_3 AEA values are within 0.1 eV of each other and the PaO_3 has the lowest AEA.

Table 5. Adiabatic Electron Affinity (AEA) of MO_3 and Vertical Detachment Energy (VDE) of MO_3^- at the FPD Level in eV.

MO_3	AEA	VDE
VO_3	3.94	4.21
NbO_3	4.02	4.54
TaO_3	4.45	4.59
PaO_3	3.76	

Wu and Wang[110] reported a vertical detachment energy (VDE) of 4.36 eV for VO_3 from a photoelectron spectroscopy study and assigned the VDE to be the AEA. They concluded that the

anion and neutral should have a similar C_{2v} geometry. However, we predict that VO_3^- is planar with D_{3h} symmetry and neutral VO_3 is nonplanar with C_s symmetry. Thus, the VDE and AEA are not likely to be the same. As the experimental band is broad, we calculated the VDE which corresponds to the transition from the ground state of VO_3^- to neutral VO_3 with the same anion geometry at the CCSD(T)/CBS level. The calculated VDE for VO_3^- is 0.27 eV higher than the AEA and is in reasonable agreement, 0.15 eV lower than the experimental value.[110] This difference is not surprising as there is likely to be some multi-reference character in the distorted VO_3 species at the anion geometry.

There is a larger predicted difference in the VDE and AEA for NbO_3, ~ 0.5 eV but for TaO_3, the difference in the AEA and VDE is smaller, < 0.15 eV. This difference is somewhat surprising given that NbO_3^- and TaO_3^- are both non-planar with C_{3v} symmetry. We were unable to calculate a VDE for PaO_3^- due to convergence issues.

Heats of Formation: Metal Fluorides As a further benchmark of our computational approach, the heats of formation of the metal fluorides were calculated at the FPD level as they can be compared to experiment.[92,93,91,111] The gas phase heats of formation at 298 K for the MF_5 were computed following the FPD composite approach described above and are given in Table 6. The calculated metal fluorides heats of formation are in general good agreement with the experimental values. The heat of formation of VF_5 is within 1 kcal/mol of the experimental value. The values calculated using the DKH3 Hamiltonian and the appropriate basis sets and ECP basis sets are essentially identical. The heat of formation of NbF_5 is predicted to be about 7 kcal/mol less negative than the experimental value. The value for TaF_5 is about 5 kcal/mol less negative than the experimentally obtained value. This suggests that the experimental values may need to be

revised. The calculated value for PaF_5 overlaps experimental value given the range of the computational (± 4 kcal/mol) and experimental error (± 12 kcal/mol) bars.

Table 6. Calculated Heats of Formation at 298K at the FPD Level for MF_5 in kcal/mol.

Species	ΣD^0_{0K}	$\Delta H_{f,0K}$	$\Delta H_{f,298K}$	$\Delta H_{f,298K}$ expt
VF_5 [a]	557.4	-342.6	-344.1	-342.7 [c]
VF_5 [b]	557.5	-342.8	-344.3	-343.25 ± 0.20 [d]
NbF_5	675.1	-408.3	-409.7	-415.8 [c] -416.50 ± 0.34 [e]
TaF_5	710.1	-431.0	-432.3	-437 ± 3 [e]
PaF_5 [f]	750.0	-521.5	-522.4	-509 ± 12 [g]

[a] DKH3 Hamiltonian and associated basis sets. [b] ECP basis sets used. [c] Ref. 90; [d] Ref. 111; [e] Ref. 91; [f] FPD heat of formation calculated as $PaF_5 \rightarrow Pa^+ + 5F + e^-$ and corrected by IE(Pa); [g] Ref. 92.

Heats of Formation: M_2O_5 The total atomization energies (TAE/ΣD_0) and gas-phase heats of formation for the M_2O_5 isomers have been calculated using the FPD approach and are listed in Table 7. For the transition metals (V, Nb, Ta), the predicted values were calculated for each isomer

Table 7. M_2O_5 Total Atomization Energies and Heats of Formation at the FPD level at 0 K and 298K in kcal/mol.

Dimer	Isomer[a]	ΣD^0_{0K}	$\Delta H_{f,0K}$	$\Delta H_{f,298K}$
V_2O_5	di-bridge	790.8	-251.1	-248.2
	tri-bridge	783.9	-244.2	-241.3
	mono-bridge	768.4	-228.7	-225.8
Nb_2O_5	di-bridge	906.0	-262.5	-264.9
	tri-bridge	903.7	-259.8	-261.2
	mono-bridge	882.5	-238.6	-240.0
Ta_2O_5	tri-bridge	935.4	-266.9	-268.5
	di-bridge	928.7	-260.2	-261.8
	mono-bridge	899.1	-230.6	-232.2
Pa_2O_5	tri-bridge	1043.5	-476.1	-477.2
	di-bridge	1030.8	-463.4	-464.5
	mono-bridge[b]	1009.2	-441.8	-442.9

[a] Atomization energy obtained by relative energies from the mono-bridge isomer. [b] FPD atomization energy calculated for this isomer as $Pa_2O_5 \rightarrow 2Pa^+ + 5O$ and corrected by the IE(Pa).

using the FPD method with respect to the atomic asymptotes of the metals. For Pa_2O_5, the atomization reaction to yield Pa^+ was used with Pa^+ in the $5f^27s^2$ configuration instead of the neutral Pa with $5f^26d^17s^2$ configuration which has many low-lying excited states.[78] The experimental IE[79] for Pa is 135.8 kcal/mol and is in good agreement with the calculated IE of 136.4 kcal/mol by Peterson and co-workers[112]. For the M_2O_5 isomers, the mono-bridge isomer was calculated at the full FPD level with the atomization energies of the other two isomers obtained from the relative energies in Table 1.

Additional Thermodynamic Quantities The cohesive energies for the M_2O_5 oxides can be calculated from the known experimental values[90] for the crystalline material: $\Delta H(V_2O_5)$ = -370.6 ± 1.5 kcal/mol; $\Delta H(Nb_2O_5)$ = -454.0 ± 1.0 kcal/mol; and $\Delta H(Ta_2O_5)$ = -489.0 ± 1.0 kcal/mol. The corresponding cohesive energies are 122.4, 189.8, and 219.6 kcal/mol, respectively.

The energetics of the dimerization of two $MO_2(OH)$ to form M_2O_5 and H_2O, Reaction (7)

$$2MO_2(OH) \rightarrow M_2O_5 + H_2O \quad (7)$$

was also examined and the enthalpy of reaction for M = V, Nb, Ta and Pa, are shown in Table 8. The heats of formation at 298 K of the $MO_2(OH)$ molecules and lowest energy isomer calculated in this work (Tables 2 and 7) and the literature $\Delta H_{f,298K}$ (H_2O) = -57.8 kcal/mol were used to predict the reaction energy. The dimerization of $TaO_2(OH)$ was predicted to be the most exothermic, followed by Pa, less exothermic by 3 kcal/mol. The dimerization of $MO_2(OH)$, M= V and Nb to form their lowest energy di-bridge structure were less exothermic by 16 and 13 kcal/mol, respectively.

Table 8. $\Delta H_{rxn,298K}$ in kcal/mol for the Reaction (7) and (8) at the FPD Level.[a]

M	Rxn 7 kcal/mol	Rxn 8 kcal/mol	Rxn 8 eV
V	-29.0	228.5	9.91
Nb	-31.8	231.6	10.04
Ta	-44.6	253.8	11.01
Pa	-41.8	202.6	8.79

[a] $\Delta H_{f,298K}(H_2O)$ = -57.8 kcal/mol. Ref. 87, 88, 89.

The energetics of the ionic dissociation of the di-bridge M_2O_5 isomer into the MO_2^+ and MO_3^- fragments, Reaction (8) was also examined and presented in Table 8. The dissociation

$$M_2O_5 \rightarrow MO_2^+ + MO_3^- \quad (8)$$

energy of the di-bridge isomer is roughly the same for V, Nb, Ta. The Pa_2O_5 isomer is the least endothermic by at most 50 kcal/mol (2 eV).

The calculated bond dissociation energies (BDEs) for the single bond M-O and double bond M=O are reported in Table 9 with experimental comparisons provided where available. The BDEs for the M=O, where calculated as half the total atomization energy of the metal dioxide, MO_2 molecule with two double bonded O, equation (9).

$$\text{BDE (M=O)} = \Sigma D^0_{0K}(MO_2)/2 \quad (9)$$

As we proceed down group 5, the BDEs increase, with Nb and Ta having similar BDEs. There is an almost 40 kcal/mol increase from the V=O to the Pa=O BDE. The BDE for PaO_2 falls within the experimental error bar of Marçalo and Gibson,[106] but is about 6 kcal/mol outside the value obtained by Kleinschmidt and Ward.[107] The higher BDE associated with Pa, is indicative of the stability of the actinyl bond in the linear PaO_2 molecule. The average M-O BDE was calculated as

half the difference of the TAE of the mono-bridge isomer and twice the TAE of the MO_2, equation (10).

$$\text{BDE (M-O)} = (\Sigma D^0_{0K}(M_2O_5) - 2x\Sigma D^0_{0K}(MO_2))/2 \quad (10)$$

The BDE for M-O for the dimers are at most 10 kcal/mol apart. The Nb and Pa have nearly identical M-O BDEs slightly higher than V by 7 kcal/mol and lower than Ta by 3 kcal/mol.

Table 9. Average M=O BDEs and M–O BDEs in kcal/mol at the FPD Level.

M	BDE(M=O) Eq. (9)	BDE (M=O) lit.	BDE(M-O) Eq. (10)
V	143		97
Nb	169		104
Ta	171		107
Pa	200	191 ± 12[106] 188.4 ± 4.1[107]	105

Electronic Structure Analysis The Natural Population Analysis (NPA) based on the Natural Bond Orbitals (NBOs)[113,114] using NBO7[115,116] for the metal oxides was calculated using Molpro 2021.1 (Supporting Information). The bonding in M_2O_5 isomers shows substantial ionic character with electron donation from the O atoms to the M.

For the transition metals, the least ionicity is predicted for V_2O_5. The V_2O_5 structures have a charge of approximately +2 on the metal, less than -1.0 on the terminal O and approximately -1.0 on the bridging O. There is substantial electron donation from the O atoms into the 3d orbitals on the V. For the fragments, there is about a charge of +2.0 on the V in VO_3^- and VO_2^+ with charges on the O of -0.5 in the latter and -1.0 in the former. For the Nb_2O_5 isomers, the bonding is more ionic with a +2.5 to 2.7 charge on the Nb so that there is less electron donation from the O atoms into the 4d as compared to V_2O_5 with electron donation into the 3d. In Ta_2O_5 the bonding is even more ionic with Ta charges of approximately +2.7 to 2.9 with even less electron donation into the

5d. Note that the electron donation in all 3 transition metals is into the *n*d orbitals with (*n*+1)s orbital occupancies less than 0.2 e.

For Pa_2O_5, the charges are similar to those for Ta_2O_5 with about a charge of +2.7 on the Pa even though the Pa isomers have actinyl character. There is a noticeable difference for the di-bridge where the two Pa charges differ by about 0.37 e in contrast to the almost equal charges for the two Ta atoms in the di-bridge structure. This arises because of the actinyl type PaO_2^+ group in the di-bridge structure. The electron donation from the O ligands to Pa in the Pa_2O_5 is completely different from that in the transition metal M_2O_5 with about one electron in the 5f and one electron in the 6d. In the mono- and tri-bridge isomers, the electron donation from the O ligands to the 5f and 6d orbitals is about equal. The Pa_2O_5 di-bridge structure shows an uneven electron donation from the O ligands into the 5f and 6d character on the Pa atoms with populations of $5f^{0.80}6d^{1.27}$ and $5f^{1.16}6d^{1.23}$. This is not surprising given the importance of the actinyl PaO_2^+ moiety in these structures.

Conclusions

The molecular geometries of select metal oxide species, MO_3^-, MO_2^+, MO_3, MO_2, $MO_2(OH)$ and M_2O_5 for M = V, Nb, Ta, Pa were predicted at the DFT/B3LYP level of theory. The MO_2^+ and MO_2, M = V, Nb, Ta, have C_{2v} symmetry, but PaO_2 and PaO_2^+ have $D_{\infty h}$ symmetry. For the MO_3, M = V, Nb, Ta, have C_s symmetry and PaO_3 has C_{2v} symmetry. The MO_3^- species for M = Nb, Ta, Pa have C_{3v} symmetry, and VO_3^- has D_{3h} symmetry. Mono-, di-, and tri-bridge isomers were optimized for M_2O_5. Single point energies at the CCSD(T) level predicted for M = V and Nb that the lowest energy isomer was the di-bridge and for M = Ta and Pa that the lowest energy isomer was the tri-bridge. The composition of the di-bridge isomers was predicted to be a combination of MO_3^- and MO_2^+ fragments. Similarly, the mono-bridge and tri-bridge isomers were

predicted to be composed of two MO_2^+ fragments linked with an O^{2-}. The NBO analysis showed that the ionicity in the bonding of the M_2O_5 molecules increases and electron donation from the O atoms to the M decreases going down the group 5 metals. The Pa_2O_5 mono- and tri-bridge isomers are similar to the Ta dimers, but there are noticeable differences in the di-bridge isomers with unequal Pa charges. The charge analysis comparison of the dimers to their MO_2^+ and MO_3^- fragments supports the ionic nature of the dimers.

The FPD method was used to calculate the TAEs and heats of formation of MO_2, MO_2^+, MO_3, MO_3^-, $MO_2(OH)$, and M_2O_5 as well as MF_5. The predicted heats of formation of the MO_2 species are in better agreement with experiment when using the PW91 orbitals as compared to the HF orbitals (see SI). The calculated IE of the transition metal oxides range from 8.0 – 8.8 eV and PaO_2 has the lowest IE of 6.25 eV. The calculated AEA ranges from 3.7 to 4.5 eV for the MO_3 species. The VDE ranges from 4.2 to 4.6 eV for the V, Nb, and Ta MO_3 species. The formation of M_2O_5 from two $MO_2(OH)$ with loss of H_2O was predicted to be the most exothermic, -45 kcal/mol, for M = Ta and the least exothermic, -29 kcal/mol, for M = V. The ionic dissociation energy of the di-bridge isomers into MO_3^- and MO_2^+, for M = V, Nb, and Ta, ranges from 10 to 11 eV and for Pa is 8.85 eV.

The energetics of the MO_2 species were used to estimate the M=O bond dissociation energies (BDEs) at the FPD level. The M=O BDEs increase as down the group. The Nb=O and Ta=O BDEs are similar, ~ 170 kcal/mol. The difference in the M=O BDE between V and Nb is ~ 25 kcal/mol and between Ta and Pa is ~ 28 kcal/mol. The BDEs of the M-O bonds can be predicted from the energetics of the mono-bridge M_2O_5. The M-O BDEs were predicted to fall in a range of about 10 kcal/mol about an average value of 100 to 105 kcal/mol.

For the M_2O_5 structures, the Pa_2O_5 clearly exhibits actinyl character in the approximately linear PaO_2^+ fragments. The electron donation from the O ligands is approximately 1 electron each into the 5f and 6d orbitals as compared to 2 electrons into the *n*d orbitals for the corresponding transition metal molecules. Thus, the Pa in Pa_2O_5 is exhibiting substantial actinide character and is clearly again in the transition region between actinide and transition metal character.

Author Contributions E. Lontchi, M. M. Mason, and M. Vasiliu performed the calculations. All authors participated in the data analysis and in writing the manuscript. D. A. D. designed the project and obtained the funding.

Conflicts of Interest There are no conflicts to declare.

Acknowledgements This work was supported by the U.S. Department of Energy (DOE), Office of Science, Office of Basic Energy Sciences, through the Heavy Element Chemistry Grant No. DE-SC0018921 for the protactinium work and for the transition metal by UNCAGE-ME, an Energy Frontier Research Center funded by the United States Department of Energy, Office of Science, Basic Energy Sciences under Award DE-SC0012577. D.A.D. thanks the Robert Ramsay Fund at The University of Alabama. We thank Dr. Gabriel de Melo for the spin orbit calculations.

Supporting Information Geometry analysis of $MO_2(OH)$; total atomization energies as a function of basis set; additional FPD corrections; TAEs and heats of formation of M_2O_5 species at the CBS Q5 limit; TaO_2 and $TaO_2(OH)$ $\Delta H_{f,0K}$ comparisons; T_1 values with HF and PW91 orbitals; NPA charges and NBO population analysis; optimized Cartesian coordinates.

ORCID

Eddy Lontchi 0000-0003-3941-289x

Marcos M. Mason: 0000-0001-9354-0409

Monica Vasiliu: 0000-0001-7573-4787

David A. Dixon: 0000-0002-9492-0056

References

[1] Y. Tokura, Optical and Magnetic Properties of Transition Metal Oxides. *Curr. Opin. Solid State Mater. Sci.* **1998,** *3,* 175-180.

[2] H. Vo, S. Zhang, W. Wang and G. Galli, Lessons Learned from First-Principles Calculations of Transition Metal Oxides. *J. Chem. Phys.* **2021,** *154,* 174704.

[3] L. J. Burcham, Briand, L. E. and I. E. Wachs, Quantification of Active Sites for the Determination of Methanol Oxidation Turn-Over Frequencies Using Methanol Chemisorption and in Situ Infrared Techniques. 1. Supported Metal Oxide Catalysts. *Langmuir*. **2001**, *17*, 6164-6174.

[4] B. M. Weckhuysen and D. E. Keller, Chemistry, Spectroscopy and the Role of Supported Vanadium Oxides in Heterogeneous Catalysis. *Catal. Today*. **2003**, *78*, 25-46.

[5] I. E. Wachs, Catalysis Science of Supported Vanadium Oxide Catalysts. *Dalton Trans.* **2013**, *42,* 11762-11769.

[6] H. S. Rosenberg, L. M. Curran, A. V. Slack, J. Ando and J. H. Oxley, Post Combustion Methods for Control of NO_x Emissions. *Prog. Energy Combust. Sci.* **1980**, *6*, 287-302.

[7] M. M. Mason, Z. R. Lee, M. Vasiliu, I. E. Wachs and D. A. Dixon, Initial Steps in the Selective Catalytic Reduction of NO with NH_3 by TiO_2-Supported Vanadium Oxides. *ACS Catal.* **2020,** *10,* 13918-3931.

[8] M. M. Mason and D. A. Dixon, Electronic Structure Investigation of NO_2 and NO Binding on Vanadium Oxides. *J. Phys. Chem. A*, **2022**, *126*, 8618-8632.

[9] M. M. Mason, I. E. Wachs and D. A. Dixon, Assignment of Vibrational Bands of Critical Surface Species Containing Nitrogen in the Selective Catalytic Reduction (SCR) of NO by NH_3. *J. Phys. Chem. C*, **2023**, *127*, 240-249.

[10] N. R. Jaegers, C. Wan, M. Y. Hu, M. Vasiliu, D. A. Dixon, E. Walter, I. E. Wachs, Y. Wang and J. Z. Hu, Investigation of Silica-Supported Vanadium Oxide Catalysts by High-field ^{51}V MAS NMR. *J. Phys. Chem. C*, **2017**, *121*, 6246–6254.

[11] N. R. Jaegers, J.-K. Lai, Y. He, E. Walter, D. A. Dixon, M. Vasiliu, Y. Chen, C. Wang, M. Y. Hu, K. T. Mueller, I. E. Wachs, Y. Wang and J. Z. Hu, Mechanism by which Tungsten Oxide Promotes the Activity of Supported V_2O_5/TiO_2 Catalysts for NO_X Abatement: Structural Effects Revealed by ^{51}V MAS NMR Spectroscopy. *Angew. Chem., Int. Ed.*, **2019**, *58*, 12609-12616.

[12] W. Weltner and D. McLeod, Spectroscopy of TaO and TaO_2 in Neon and Argon Matrices at 4° and 20°K. *J. Chem. Phys*. **1965**, *42*, 882-891.

[13] M. Zhou and L. Andrews, Reactions of Laser-Ablated Niobium and Tantalum Atoms with Oxygen Molecules: Infrared Spectra of Niobium and Tantalum Oxide Molecules, Anions, and Cations. *J. Phys. Chem. A*. **1998**, *102*, 8251-8260.

[14] W. W. Albrecht, Production, Properties and Application of Tantalum, Niobium and Their Compounds. In *Lanthanides, Tantalum and Niobium: Mineralogy, Geochemistry, Characteristics of Primary Ore Deposits, Prospecting, Processing and Applications*; Möller, P., Černy, P., Saupé, F. Eds.; Springer-Verlag, 1989; pp 345-358.

[15] N. N. Greenwood and A. Earnshaw, *Chemistry of the Elements*, 2nd ed; Butterworth-Heinemann, 1998.

[16] S. Pérez-Walton, C. Valencia-Balvín, G. M. Dalpian and J. M. Osorio-Guillén, Electronic, Dielectric, and Optical Properties of the B Phase of Niobium Pentoxide and Tantalum Pentoxide by First-Principles Calculations Phys. *Status Solidi B* **2013,** *15,* 1352-1357.

[17] A. M. Raba, J. Bautista-Ruíz and M. R. Joya, Synthesis and Structural Properties of Niobium Pentoxide Powders: A Comparative Study of the Growth Process. *Mater. Res* **2016**, *19*, 1381-1387.

[18] H. S. Hong and K. S. Lee, Thermodynamic Evaluation of the Ta-O System from Pure Tantalum to Tantalum Pentoxide. *J. Alloys Compd.* **2003**, *360,* 198-204.

[19] K. T. Jacob, C. Shekhar and Y. Waseda, An Update on the Thermodynamics of Ta_2O_5. *J. Chem. Thermodyn.* **2009,** *41,* 748-753.

[20] L. R. Morss, N. M. Edelstein, J. Fuger and J. J. Katz, *The Chemistry of the Actinides and Transactinide Elements;* Springer: Dordrecht, The Netherlands, 2006.

[21] X. Wen, R. L. Martin, L. E. Roy, G. E. Scuseria, S. P. Rudin, E. R. Batista, T. M. McCleskey, B. L. Scott, E. Bauer, J. J. Joyce and T. Durakiewicz, Effect Of Spin-Orbit Coupling on the Actinide Dioxides AnO_2 (An=Th, Pa, U, Np, Pu, and Am): A Screened Hybrid Density Functional Study. *J. Chem. Phys.* **2012,** *137,* 154707.

[22] R. E. Wilson, S. De Sio and V. Vallet, Protactinium and The Intersection of Actinide and Transition Metal Chemistry. *Nat. Commun.* **2018**, *9*, 622.

[23] B. Siberchicot and J. Aupiais, Prediction of Structural Properties of Protactinium Pentoxide Pa_2O_5 by First-Principles Calculations. *Mater. Res. Express* **2018,** *5,* 105903.

[24] T. Liu, S. Li, T. Gao and B. Y. Ao, Theoretical Prediction of Some Layered Pa_2O_5 Phases: Structure and Properties. *RSC Adv.* **2019,** *9,* 31398-31405.

[25] T. Liu, S. Li, T. Gao and B. Y. Ao, Density Functional Investigation of Fluorite-based Pa_2O_5 Phases: Structure and Properties. *Chin. J. Phys.* **2020,** *64,* 115-122.

[26] H. T. Deng, K. P Kerns and A. W. Castleman, Formation, Structures, and Reactivities of Niobium Oxide Cluster Ions. *J. Phys. Chem.* **1996,** *100,* 13386-13392.

[27] S. F. Vyboishchikov and J. Sauer, $(V_2O_5)_n$ Gas-Phase Clusters (n = 1 – 12) Compared to V_2O_5 Crystal: DFT Calculations. *J. Phys. Chem. A* **2001**, *105,* 8588-8598.

[28] S. F. Vyboishchikov and J. Sauer, Gas-Phase Vanadium Oxide Anions: Structure and Detachment Energies from Density Functional Calculations. *J. Phys. Chem. A* **2000,** *104,* 10913-10922.

[29] M. Calatayud, J. Andrés and A. A Beltrán, Systematic Density Functional Theory Study of $V_xO_y^+$ and V_xO_Y (X = 2-4, Y = 2-10) Systems. *J. Phys. Chem. A.* **2001,** *105,* 9760-9775.

[30] A. Kovács, Molecular Oxides of High-Valent Actinides. *Struct. Chem.* **2020,** *31,* 1247-1271.

[31] S. Li and D. A. Dixon, Benchmark Calculations on the Electron Detachment Energies of MO_3^- and $M_2O_6^-$ (M = Cr, Mo, W). *J. Phys. Chem. A*. **2007**, *111*, 11908-11921.

[32] S. Li and D. A. Dixon, Molecular Structures and Energetics of the $(TiO_2)_n$ (n = 1–4) Clusters and Their Anions. *J. Phys. Chem. A*. **2008**, *112*, 6646-6666.

[33] S. Li, J. M. Hennigan, D. A. Dixon and K. A. Peterson, Accurate Thermochemistry for Transition Metal Oxide Clusters. *J. Phys. Chem. A*. **2009**, *113*, 7861-7877.

[34] R. Craciun, R. T. Long, D. A. Dixon and K. O. Christe, Electron Affinities, Fluoride Affinities, and Heats of Formation of the Second Row Transition Metal Hexafluorides: MF_6 (M = Mo, Tc, Ru, Rh, Pd, Ag). *J. Phys. Chem. A*. **2010**, *114*, 7571-7582.

[35] R. Craciun, D. Picone, R. T. Long, S. Li, D. A. Dixon, K. A. Peterson and K. O. Christe, Third Row Transition Metal Hexafluorides, Extraordinary Oxidizers, and Lewis Acids: Electron

Affinities, Fluoride Affinities, and Heats of Formation of WF_6, ReF_6, OsF_6, IrF_6, and AuF_6. *Inorg. Chem*. **2010**, *49*, 1056-1070.

[36] Z. Fang, J. Both, S. Li, S. Yue, E. Aprà, M. Keçeli, A. F. Wagner and D. A. Dixon, Benchmark Calculations of Energetic, Properties of Groups 4 and 6 Transition Metal Oxide Nanoclusters Including Comparison to Density Functional Theory. *J. Chem. Theory Comput*. **2016**, *12*, 3689-3710.

[37] Z. Fang, Z. Lee, K. A. Peterson and D. A. Dixon, Use of Improved Orbitals for CCSD(T) Calculations for Predicting Heats of Formation of Group IV and Group VI Metal Oxide Monomers and Dimers and UCl_6. *J. Chem. Theory Comput*. **2016**, *12*, 3583-3592.

[38] D. Feller, K. A. Peterson and D. A. Dixon, A Survey of Factors Contributing to Accurate Theoretical Predictions of Atomization Energies and Molecular Structures. *J. Chem. Phys*. **2008**, *129*, 204105.

[39] D. A. Dixon, D. Feller and K. A. Peterson, A Practical Guide to Reliable First Principles Computational Thermochemistry Predictions across the Periodic Table. In Annual Reports in Computational Chemistry; Wheeler, R. A., Tschumper, G., Eds.; Elsevier: Amsterdam, 2012; Vol. *8*, pp 1-28.

[40] D. Feller, K. A. Peterson and D. A. Dixon, Further Benchmarks of a Composite, Convergent, Statistically Calibrated Coupled-Cluster- Based Approach for Thermochemical and Spectroscopic Studies *Mol. Phys*. **2012**, *110*, 2381-2399.

[41] K. A. Peterson, D. Feller and D. A. Dixon, Chemical Accuracy in Ab Initio Thermochemistry and Spectroscopy: Current Strategies and Future Challenges. *Theor. Chem. Acc*. **2012**, *131*, 1-20.

[42] D. Feller and D. A. Dixon, Extended Benchmark Studies of Coupled Cluster Theory through Triple Excitations. *J. Chem. Phys*. **2001**, *115*, 3484-3496.

[43] R. G. Parr and W. Yang, *Density-Functional Theory of Atoms and Molecules*; Oxford University Press: New York, 1989.

[44] C. Lee, W. Yang and R. G. Parr, Development of the Colle-Salvetti Correlation-Energy Formula into a Functional of the Electron Density. *Phys. Rev. B.* **1988**, *37*, 785-789.

[45] A. D. Becke, Density-Functional Thermochemistry. III. The Role of Exact Exchange. *J. Chem. Phys.* **1993**, *98*, 5648-5652.

[46] W. Kohn, A. D. Becke and R. G. Parr, Density Functional Theory of Electronic Structure. *J. Phys. Chem.* **1996**, *100*, 12974-12980.

[47] T. H. Dunning, Gaussian Basis Set for Use in Correlated Molecular Calculations. I. The Atoms Boron Through Neon and Hydrogen. *J. Chem. Phys*. **1989**, *90*, 1007-1023.

[48] R. A. Kendall, T. H. Dunning and R. J. Harrison, Electron Affinities of the First-Row Atoms Revisited. Systematic Basis Sets and Wave Functions. *J. Chem. Phys*. **1992**, *96*, 6796-6806.

[49] D. E. Woon and T. H. Dunning, Gaussian Basis Sets for Use in Correlated Molecular Calculations. III. The Atoms Aluminum through Argon. *J. Chem. Phys*. **1993**, *98*, 1358-1371.

[50] S. Li, J. M. Hennigan, D. A. Dixon and K. A. Peterson, Accurate Thermochemistry for Transition Metal Oxide Clusters. *J. Phys. Chem. A* **2009,** *113,* 7861-7877.

[51] K. A. Peterson, D. Figgen, M. Dolg and H. Stoll, Energy-Consistent Relativistic Pseudopotentials and Correlation Consistent Basis Sets for the *4d* Elements Y–Pd. *J. Chem. Phys*. **2007**, *126*, 124101.

[52] D. Figgen, K. A. Peterson, M. Dolg and H. Stoll, Energy-consistent Pseudopotentials and Correlation Consistent Basis Sets for the 5*d* Elements Hf-Pt. *J. Chem. Phys*. **2009**, *130*, 164108.

[53] M. Vasiliu, K. A. Peterson, J. K. Gibson and D. A. Dixon, Reliable Potential Energy Surfaces for the Reactions of H_2O with ThO_2, PaO_2^+, UO_2^{2+}, and UO_2^+. *J. Phys. Chem. A*. **2015**, *119*, 11422-11431.

[54] A. Weigand, X Cao, T. Hangele and M. Dolg, Relativistic Small-Core Pseudopotentials for Actinium, Thorium, and Protactinium. *J. Phys. Chem. A*. **2014**, *118*, 2519-2530.

[55] M. J. Frisch, G. W. Trucks, H. B. Schlegel, G. E. Scuseria, M. A. Robb, J. R. Cheeseman, G. Scalmani, V. Barone, G. A. Petersson, H. Nakatsuji, X. Li, M. Caricato, A. V. Marenich, J. Bloino, B. G. Janesko, R. Gomperts, B. Mennucci, H. P. Hratchian, J. V. Ortiz, A. F. Izmaylov, J. L. Sonnenberg, D. Williams-Young, F. Ding, F. Lipparini, F. Egidi, J. Goings, B. Peng, A. Petrone, T. Henderson, D. Ranasinghe, V. G. Zakrzewski, J. Gao, N. Rega, G. Zheng, W. Liang, M. Hada, M. Ehara, K. Toyota, R. Fukuda, J. Hasegawa, M. Ishida, T. Nakajima, Y. Honda, O. Kitao, H. Nakai, T. Vreven, K. Throssell, J. A. Montgomery Jr., J. E. Peralta, F. Ogliaro, M. J. Bearpark, J. J. Heyd, E. N. Brothers, K. N. Kudin, V. N. Staroverov, T. A. Keith, R. Kobayashi, J. Normand, K. Raghavachari, A. P. Rendell, J. C. Burant, S. S. Iyengar, J. Tomasi, M. Cossi, J. M. Millam, M. Klene, C. Adamo, R. Cammi, J. W. Ochterski, R. L. Martin, K. Morokuma, O. Farkas, J. B. Foresman and D. J. Fox, *Gaussian 16, Revision C.01*, Gaussian, Inc., Wallingford CT, 2016.

[56] G. D. Purvis and R. J. Bartlett, A Full Coupled-Cluster Singles and Doubles Model: The Inclusion of Disconnected Triples. *J. Chem. Phys.* **1982**, *76*, 1910-1918.

[57] K. Raghavachari, G. W. Trucks, J. A. Pople and M. Head-Gordon, A Fifth-order Perturbation Comparison of Electron Correlation Theories. *Chem. Phys. Lett.* **1989**, *157*, 479-483.

[58] J. D. Watts, J. Gauss and R. J. Bartlett, Coupled-cluster Methods with Noniterative Triple Excitations for Restricted Open-shell Hartree–Fock and Other General Single Determinant Reference Functions. Energies and Analytical Gradients. *J. Chem. Phys.* **1993**, *98*, 8718-8733.

[59] R. J. Bartlett and M. Musiał, Coupled-Cluster Theory in Quantum Chemistry. *Rev. Mod. Phys.* **2007**, *79*, 291-352.

[60] J. P. Perdew and Y. Wang, Accurate and Simple Analytic Representation of the Electron-Gas Correlation Energy. *Phys. Rev. B: Condens. Matter Mater. Phys.* **1992**, *45*, 13244-13249.

[61] J. P. Perdew, K. Burke and Y. Wang, Generalized Gradient Approximation for the Exchange-Correlation Hole of a Many-Electron System. *Phys. Rev. B: Condens. Matter Mater. Phys.* **1996**, *54*, 16533-16539.

[62] K. Burke, J. P. Perdew and Y. Wang, Derivation of a Generalized Gradient Approximation: The PW91 Density Functional. In *Electronic Density Functional Theory: Recent Progress and New Directions*; Dobson, J. F., Vignale, G., Das, M. P., Eds.; Plenum: New York, 1997; pp 81-122.

[63] M. J. O. Deegan and P. J. Knowles, Perturbative Corrections to Account for Triple Excitations in Closed and Open Shell Coupled Cluster Theories. *Chem. Phys. Lett.* **1994**, *227*, 321-326.

[64] M. Rittby and R. J. Bartlett, An Open-Shell Spin-Restricted Coupled Cluster Method: Application to Ionization Potentials in N_2. *J. Phys. Chem*. **1988**, *92*, 3033-3036.

[65]P. J. Knowles, C. Hampel and H.-J. Werner, Coupled Cluster Theory for High Spin, Open Shell Reference Wave Functions. *J. Chem. Phys.* **1993**, *99*, 5219-5228.

[66] H.-J. Werner, P. J. Knowles, G. Knizia, F. R. Manby and M. Schütz, Molpro: A General-Purpose Quantum Chemistry Program Package. *WIREs Comput. Mol. Sci*. **2012**, *2*, 242-253.

[67] H.-J. Werner, P. J. Knowles, F. R. Manby, J. A. Black, K. Doll, A. Heßelmann, D. Kats, A. Köhn, T. Korona, D. A. Kreplin, Q. Ma, T. F. Miller, III, A. Mitrushchenkov, K. A. Peterson, I. Polyak, G. Rauhut and M. Sibaev, The Molpro Quantum Chemistry Package. *J. Chem. Phys.* **2020**, *152*, 144107.

[68] H.-J. Werner, P. J. Knowles, G. Knizia, F. R. Manby, M. Schütz, P. Celani, W. Györffy, D. Kats, T. Korona, R. Lindh, A. Mitrushenkov, G. Rauhut, K. R. Shamasundar, T. B. Adler, R. D. Amos, S. J. Bennie, A. Bernhardsson, A. Berning, D. L. Cooper, M. J. O. Deegan, A. J. Dobbyn, F. Eckert, E. Goll, C. Hampel, A. Hesselmann, G. Hetzer, T. Hrenar, G. Jansen, C. Köppl, S. J. R. Lee, Y. Liu, A. W. Lloyd, Q. Ma, R. A. Mata, A. J. May, S. J. McNicholas, W. Meyer, T. F. Miller III, M. E. Mura, A. Nicklass, D. P. O'Neill, P. Palmieri, D. Peng, T. Petrenko, K. Pflüger, R. Pitzer, M. Reiher, T. Shiozaki, H. Stoll, A. J. Stone, R. Tarroni, T. Thorsteinsson, M. Wang, and M. Welborn, *MOLPRO, version 2018.2, a package of ab initio programs*, See http://www.molpro.net. Accessed August 1, 2022.

[69] K. A. Peterson, D. E. Woon and T. H. Dunning, Benchmark Calculations with Correlated Molecular Wave Functions. IV. The Classical Barrier Height of the $H+H_2 \rightarrow H_2+H$ Reaction. *J. Chem. Phys.* **1994**, *100*, 7410-7415.

[70] M. Douglas and N. M. Kroll, Quantum Electrodynamical Corrections to the Fine Structure of Helium. *Ann. Phys.* **1974**, *82*, 89-155.

[71] B. A. Hess, Applicability of the No-pair Equation with Free-Particle Projection Operators to Atomic and Molecular Structure Calculations. *Phys. Rev. A: At., Mol., Opt. Phys*. **1985**, *32*, 756-763.

[72] Hess, B. A. Relativistic Electronic-Structure Calculations Employing a Two-Component No-Pair Formalism with External-Field Projection Operators. *Phys. Rev.* **1986**, *33*, 3742−3748.

[73] N. B. Balabanov and K. A. Peterson, Systematically Convergent Basis Sets for Transition Metals. I. All-Electron Correlation Consistent Basis Sets for the *3d* Elements Sc-Zn. *J. Chem. Phys*. **2005**, *123*, 064107.

[74] W. A de Jong, R. J. Harrison and D. A Dixon, Parallel Douglas-Kroll Energy and Gradients in NWChem: Estimating Scalar Relativistic Effects Using Douglas-Kroll Contracted Basis Sets. *J. Chem. Phys*. **2001**, *114*, 48-53.

[75] K. A. Peterson and T. H. Dunning, Accurate Correlation Consistent Basis Sets for Molecular Core-Valence Correlation Effects: The Second Row Atoms Al-Ar, and the First Row Atoms B-Ne Revisited. *J. Chem. Phys.* **2002**, *117*, 10548-10560.

[76] C. E. Moore, *Atomic Energy Levels as Derived from the Analysis of Optical Spectra, Vol. 1, H to V*; U.S. National Bureau of Standards Circular 467; U.S. Department of Commerce, National Technical Information Service: Washington, D.C., 1949; COM-72-50282.

[77] C. E. Moore, *Atomic Energy Levels as Derived from the Analysis of Optical Spectra, Vol. 2, Cr to Nb*; U.S. National Bureau of Standards Circular 467, U.S. Department of Commerce, National Technical Information Service: Washington, D.C., 1949; COM-72-50216.

[78] J. E. Sansonetti and W. C. Martin, Handbook of Basic Atomic Spectroscopic Data. *J. Phys. Chem. Ref. Data*. **2005**, *34*, 1559-2259.

[79] A. Kramida, Y. Ralchenko, J. Reader, and NIST ASD Team (2021). *NIST Atomic Spectra Database* (version 5.9), [Online]. Available: http://physics.nist.gov/asd, Accessed August 11, 2022. National Institute of Standards and Technology, Gaithersburg, MD.

[80] K. Andersson, P. A. Malmqvist, B. O. Roos, A. J. Sadlej and K. Wolinski, Second-Order Perturbation Theory with a CASSCF Reference Function. *J. Phys. Chem.* **1990**, *94*, 5483-5488.

[81] K. Andersson, P. A. Malmqvist and B. O. Roos, Second-Order Perturbation Theory with a Complete Active Space Self-Consistent Field Reference Function. *J. Chem. Phys.* **1992**, *96*, 1218-1226.

[82] A. Berning, M. Schweizer, H.-J. Werner, P. J Knowles and P. Palmieri, Spin-orbit Matrix Elements for Internally Contracted Multireference Configuration Interaction Wavefunctions. *Mol. Phys.* **2000**, *98*, 1823-1833.

[83] A. Wolf, M. Reiher and B. A. Hess, The Generalized Douglas-Kroll Transformation. *J. Chem. Phys.* **2002**, *117*, 9215-9226.

[84] G. F. de Melo, M. Vasiliu, M. Marshall, Z. Zhu, B. A. Tufekci, S. M. Ciborowski, M. Blankenhorn, R. M. Harris, K. H. Bowen and D. A. Dixon, Experimental and Computational Description of the Interaction of H and H^- with U. *J. Phys. Chem. A*, **2022**, *126*, 4432-4443.

[85] G. F. de Melo D. A. Dixon, Protactinium and Actinium Monohydrides: A Theoretical Study on Their Spectroscopic and Thermodynamic Properties. *J. Phys. Chem. A*, **2022**, *126*, 6171-6184.

[86] G. F. de Melo, M. Vasiliu, G. Liu, S. Ciborowski, Z. Zhu, M. Blankenhorn, R. Harris, C. Martinez-Martinez, M. Dipalo, K. A. Peterson, K. H. Bowen and D. A Dixon, Electronic Properties of UN and UN^- from Photoelectron Spectroscopy and Correlated Molecular Orbital Theory. *J. Phys. Chem. A*, **2022**, *126,* 7944-7953.

[87] B. Ruscic, R. E. Pinzon, M. L. Morton, G. von Laszewski, S. J. Bittner, S. G. Nijsure, K. A. Amin, M. Minkoff and A. F. Wagner, Introduction to Active Thermochemical Tables: Several "Key" Enthalpies of Formation Revisited. *J. Phys. Chem. A* **2004**, *108*, 9979-9997.

[88] P. B. Changala, T. L. Nguyen, J. H. Baraban, G. B. Ellison, J. F. Stanton, D. H. Bross and B. Ruscic, Active Thermochemical Tables: The Adiabatic Ionization Energy of Hydrogen Peroxide. *J. Phys. Chem. A* **2017**, *121*, 8799-8806.

[89] B. Ruscic and D. H. Bross, *Active Thermochemical Tables (ATcT)*, version 1.122; Argonne National Laboratory: Argonne, IL, 2019.

https://atct.anl.gov/Thermochemical%20Data/version%201.122g/index.php (accessed September 18, 2022).

[90] M. W. Chase, NIST-JANAF Thermochemical Tables, 4th ed. *J. Phys. Chem. Ref. Data, Monogr.* **1998,** No. 9, Suppl. 1.

[91] V. S. Yungman, V. P. Glushko, V. A. Medvedev and L. V. Gurvich, Eds.; *Thermal Constants of Substances*, 8 Vols.; Wiley: New York, 1999.

[92] R. J. M. Konings, L. R. Morss, and J. Fuger Thermodynamic Properties of Actinides and Actinide Compounds. in *The Chemistry of the Actinide and Transactinide Elements; 3rd Ed.*; Morss, L. R., Edelstein, N. M., Fuger, J., Eds.; Springer: Dordrecht, The Netherlands, **2006**; Vol. 4; Ch. 19, pp 2113-2224.

[93] D. D. Wagman, W. H. Evans, V. B. Parker, R. H. Schumm, I. Halow, S. M. Bailey, K. L. Churney and R. L. Nuttall. *J. Phys. Chem. Ref. Data, Suppl.,* **1982,** *11,* Suppl. 2.

[94] L. A. Curtiss, K. Raghavachari, P. C. Redfern and J. A. Pople, Assessment of Gaussian-2 and Density Functional Theories for the Computation of Enthalpies of Formation. *J. Chem. Phys*. **1997**, *106*, 1063-1079.

[95] E. M. Lontchi, M. Vasiliu, L. M. Tatina, A. C. Caccamo, A. N. Gomez, J. K. Gibson and D. A. Dixon, Hydrolysis of Small Oxo/Hydroxo Molecules Containing High Oxidation State Actinides (Th, Pa, U, Np, Pu): A Computational Study. *J. Phys. Chem. A* **2021,** *125,* 6158-6170.

[96] M. Vasiliu, K. A. Peterson and D. A. Dixon, Calculated Ionization Potentials of MO_3 and MO_2 for M = U, Mo, W, and Nd. *J. Phys. Chem. A* **2020,** *124,* 6913-6919.

[97] N. K. Dzhemilev, S. F. Kovalenko, S. E. Maksimov, O. F. Tukfatullin and S. T. Khojiev, Fragmentation Processes of Vanadium and Niobium Oxide Clusters Sputtered by Ion Bombardment. *J. Surf. Investig.. X-ray, Synch,. and Neutron Techniques.* **2014,** *8,* 254-258.

[98] J. W. J. Wu, R. Moriyama, M. Nakano, K. Ohshimo and F. Misaizu, Compositions and Structures of Niobium Oxide Cluster Ions, $Nb_mO_n^{\pm}$, (m = 2–12), Revealed by Ion Mobility Mass Spectrometry. *Phys. Chem. Chem. Phys.* **2017,** *19*, 24903-24914.

[99] R. Feng, E. D. Glendening, and K. A. Peterson, Actinyl Cation–Cation Interactions in the Gas Phase: An Accurate Thermochemical Study, *Phys.Chem.Chem.Phys.,* **2019**, *21*, 7953-7964.

[100] B. Vlaisavljevich, P. Mir, D. Ma, G. E. Sigmon, P. C. Burns, C. J. Cramer, and L. Gagliardi. Synthesis and Characterization of the First 2D Neptunyl Structure Stabilized by Side-on Cation–Cation Interactions. Chem. Eur. J. 2013, 19, 2937 – 2941

[101] Y. Hu, A. M. Chaka, and D. A Dixon, Thermodynamics of the Metal Carbonates and Bicarbonates of Mn, Co, Ni, Cu, and Zn Relevant to Mineral Energetics. *J. Phys. Chem. A*, **2022**, *126*, 7874-7887.

[102] C. W. Bauschlicher, N. S. Jacobson and D. L Myers, Quantum Chemical Calculations of the Thermochemistry of Tantalum Oxyhydroxide Species. *J. Am. Ceram. Soc.* **2019,** *102,* 3836-3842.

[103] J. M. L. Martin, Ab Initio Total Atomization Energies of Small Molecules - Towards the Basis Set Limit. *Chem. Phys. Lett.* **1996**, *259*, 669-678.

[104] D. Feller, K.A. Peterson and J. G. Hill, On the Effectiveness of CCSD(T) Complete Basis Set Extrapolations for Atomization Energies. *J. Chem. Phys.* **2011***, 135,* 044102-1-044102-18.

[105] S. Smoes, J. Drowart and C. E. Myers, Determination of the Atomization Energies of the Molecules TaO(g) And TaO_2(g) By the Mass-Spectrometric Knudsen-Cell Method. *J. Chem. Thermodyn.* **1976,** *8,* 255-239.

[106] J. Marçalo and J. K. Gibson, Gas-Phase Energetics of Actinide Oxides: An Assessment of Neutral and Cationic Monoxides and Dioxides from Thorium to Curium. *J. Phys. Chem. A* **2009,** *113,* 12599-12606.

[107] P. D. Kleinschmidt and J. W. Ward, Thermochemical Studies on the Plutonium Fluorides and Protactinium Oxides. *J. Less-Common Met.* **1986,** *121,* 61-66.

[108] S. L. Bennett, S.-S. Lin and P. W. Gilles, High-Temperature Vaporization of Ternary Systems. I. Mass Spectrometry of Oxygen-Rich Vanadium-Tungsten-Oxygen Species. *J. Phys. Chem.* **1974,** *78,* 266-273.

[109] M. Farber, O. M. Uy and R. D. Srivastava, Effusion-Mass Spectrometric Determination of the Heats of Formation of the Gaseous Molecules V_4O_{10}, V_4O_8, VO_2, and VO. *J. Chem. Phys.* **1972,** *56,* 5312-5315.

[110] H. Wu and L.-S. Wang, A Photoelectron Spectroscopic Study of Monovanadium Oxide Anions (VO_x^-, x=1-4). *J. Chem. Phys.* **1998,** *108,* 5310-5318.

[111] G. Johnson and W. Hubbard, The Enthalpy of Formation of Vanadium Pentafluoride By Fluorine Bomb Calorimetry. *J. Chem. Thermodyn.* **1974**, 6, 59-63.

[112] R. Feng and K. A. Peterson, Correlation Consistent Basis Sets for Actinides. II. The Atoms Ac and Np-Lr. *J. Chem. Phys.* **2017,** *147,* 084108.

[113] A. E. Reed, L. A. Curtiss and F. Weinhold, Intermolecular Interactions from a Natural Bond Orbital, Donor-Acceptor Viewpoint. *Chem. Rev.* **1988,** *88,* 899-926.

[114] F. Weinhold and C. R. Landis, *Valency and Bonding: A Natural Bond Orbital Donor-Acceptor Perspective;* University Press: Cambridge, U.K., 2005.

[115] E. D. Glendening, J. K. Badenhoop, A. E. Reed, J. E. Carpenter, J. A. Bohmann, C. M. Morales, P. Karafiloglou, C. R. Landis and F. Weinhold, *Natural Bond Order 7.0;* Theoretical Chemistry Institute, University of Wisconsin: Madison, WI, 2018. http://nbo6.chem.wisc.edu/.

[116] E. D. Glendening, C. R. Landis and F. Weinhold, NBO 7.0: New Vistas in Localized and Delocalized Chemical Bonding Theory. *J. Comput. Chem.* **2019**, *40*, 2234-2241.